VSP

Advanced Composite Materials 18 (2009) 121–134

ADVANCED COMPOSITE MATERIALS
www.brill.nl/acm

Improvement of Out-of-Plane Impact Damage Resistance of CFRP Due to Through-the-Thickness Stitching

Akinori Yoshimura [a,*], **Tomoaki Nakao** [b] **and Nobuo Takeda** [b]

[a] Advanced Materials Group, Aerospace Research and Development Directorate (ARD), Japan Aerospace Exploration Agency (JAXA), 6-13-1 Osawa, Mitaka, Tokyo 181-0015, Japan

[b] Graduate school of Frontier Sciences, The University of Tokyo, 5-1-5 Kashiwanoha, Kashiwa, Chiba 277-8561, Japan

Received 12 March 2008; accepted 18 April 2008

Abstract

The present study investigated, both experimentally and numerically, the improvement of low-velocity impact damage resistance of carbon fiber reinforced plastic (CFRP) laminates due to through-the-thickness stitching. First, we conducted drop-weight impact tests for stitched and unstitched laminates. The results of damage inspection confirmed that stitching did improve the impact damage resistance, and revealed that the improvement effect became greater as the impact energy increased. Moreover, the stitching affected the through-the-thickness damage distribution. Next, we performed FEM analysis and calculated the energy release rate of the delamination crack using the virtual crack closure technique (VCCT). The numerical results revealed that the stitching affected the through-the-thickness damage distribution because the stitch threads had a marked effect on decreasing both the modes I and II energy release rate around the bottom of the laminate. Comparison of the results for models that contained delaminations of various sizes revealed that the energy release rate became lower as delamination size increased; therefore the stitching improved the impact resistance more effectively when the impact energy was higher.

Keywords

Stitched laminate composite, damage, low-velocity impact, finite element analysis, delamination

1. Introduction

Generally, out-of-plane impact load easily generates delamination in conventional CFRP laminates because of their low interlaminar fracture toughness. Delamination significantly degrades various material properties of CFRP including tensile strength, compressive strength, fatigue life, etc. Among these, compressive strength is seriously reduced by delamination. Residual compressive strength after impact

* To whom correspondence should be addressed. E-mail: yoshimura.akinori@jaxa.jp
Edited by JSCM

 DOI:10.1163/156855109X428727

load (CAI strength: compression after impact strength) is often reduced to less than half of the compressive strength of the intact laminate. Therefore, it is essential to suppress the out-of-plane impact damage when the FRP laminates are used as the structural components that may be subjected to impact load.

Stitched CFRP laminate is a kind of three-dimensional reinforced composite, in which stitch threads are embedded along the through-the-thickness direction [1]. The stitch threads survive after the onset of delamination, and the threads bridge the delamination crack. Therefore, the apparent interlaminar fracture toughnesses of stitched laminates, which are measured by DCB (double cantilever beam) and ENF (end notched flexure) tests, are much higher than those of unstitched laminates [1–11].

Therefore, the expectation has been that stitched laminates will have high impact damage resistance. Numerous studies have conducted out-of-plane impact tests for stitched laminates, and most of the results confirmed that the out-of-plane stitching improved the impact damage resistance of the CFRP laminates [6, 10, 12–16]. However, stitching did not always greatly improve the impact damage resistance; the results presented varying degrees of improvement. Moreover, some results showed that the stitching had no effect on the impact resistance of the laminates [5]. Therefore, further discussions on the mechanism of the improvement effect of the impact damage resistance are required.

The present study, both experimentally and numerically, investigates the out-of-plane impact damage in stitched laminates, and the results reveal the effects of the stitching on the out-of-plane impact damage resistance of CFRP laminates. The present paper is organized as follows. First, in Section 2, drop-weight impact tests and detailed damage observations by NDI techniques are conducted for both stitched and unstitched laminates. In Section 3, we perform numerical simulations based on the FEA and reveal the effect of stitching on the impact damage resistance of CFRP. We then discuss the reason for the varying degrees of damage resistance improvement found in the literature.

2. Experimental

2.1. Experimental Procedure

In this research, carbon-fiber stitched CFRP laminates (Toyota Industries Corp.) were used. T800-12kf tows (Toray Industries Inc.) were used as the in-plane tows, and TR40-2kf yarns (Mitsubishi Rayon Co. Ltd.) were employed as the stitch threads. The stacking sequence of the in-plane tows was $[-45/0/45/90]_{3s}$. Figure 1 shows the stitching pattern. Stitch threads ran along the 0° direction of the in-plane tows; stitch threads and selvage yarns crossed at right-angles around the surface [17]. The stitch space and the stitch pitch were both 3.0 mm. For comparison, unstitched preform was also prepared. The fabrication procedure of the unstitched preform was the same as that of the stitched preform without the stitching process. The materials were impregnated and molded using the resin transfer molding (RTM)

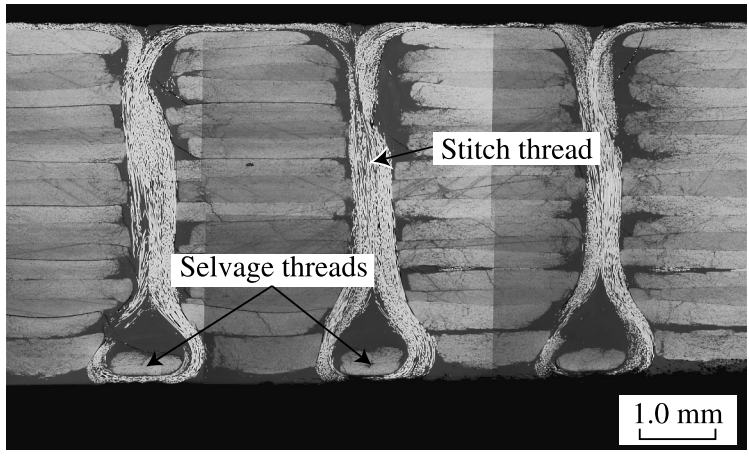

Figure 1. Cross-section of the laminate along a stitch thread.

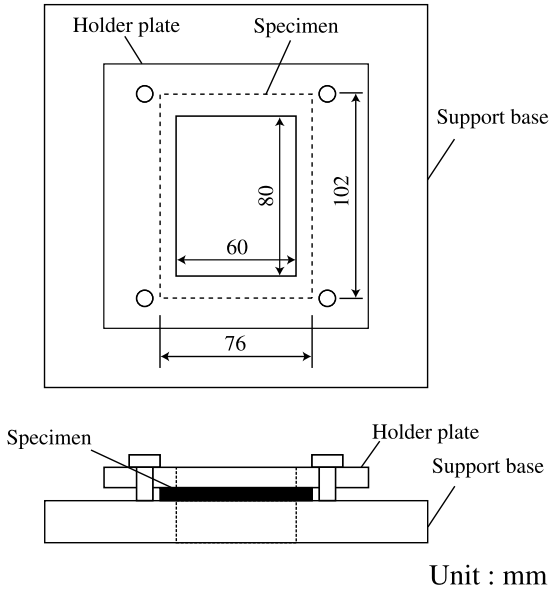

Figure 2. Schematic of the fixture used in the drop-weight impact test.

method. For the matrix, an epoxy resin system (Araldite LY5052/Aradur5052) was employed. Materials were cut by diamond saw to make rectangular specimens. The dimensions of the specimens were 102 mm in length and 76 mm in width, where the length direction was parallel to the 0° direction of the in-plane tows. The thickness of the specimens was about 4.5 mm.

A drop-weight impact test device (Instron/Dynatup 9250HV) was employed for the impact tests. Specimens were clamped using a picture frame-type holder plate and support base as shown in Fig. 2. The holder plate and support base had the same

rectangularly shaped windows; the dimensions were 80 mm × 60 mm. The impact load was applied at the center of the rectangle. The weight of the impactor was 5.07 kg, and the tip shape of the impactor was a hemisphere 12.7 mm in diameter. Three levels of impact energy were applied to each type of specimen: 0.8375, 1.675 and 3.350 J/mm, where the impact energy was normalized by the plate thickness. At least two specimens were tested at each impact energy level.

Two kinds of soft X-ray NDI were conducted for detailed observation of the impact damage. To ensure clear observation, the specimen was penetrated with contrast medium (zinc iodide) before inspection. For all specimens, we took soft X-ray radiographs using a general-purpose soft X-ray film device (M-100S, Softex, Inc.) in order to observe the in-plane distribution of the damage. For the specimens subjected to a 1.675 J/mm impact, we took section images using a soft X-ray micro-focus computed tomography (CT) system (TOSCANER-30000μhd, Toshiba IT and Control Systems Corp.) in order to observe through-the-thickness distribution of the damage.

2.2. Experimental Results

Figure 3 shows the soft X-ray radiographs of the specimens. The damaged area in the stitched specimen was always smaller than that in the unstitched specimen for the same level of energy. In the unstitched specimens, one long, straight ply crack always occurred in the $-45°$ ply at the bottom of the specimen, and the impact damage spread along the $-45°$ crack. However, although ply cracks occurred in the stitched specimens, the cracks did not extend as far as those in the unstitched specimens. The impact damage expanded relatively equally in all directions.

Figure 4 plots the projected damage area as a function of the impact energy, where the areas were obtained by processing the X-ray radiograph images digitally. When the impact energy was low, the difference in the damaged areas between the stitched and unstitched specimens was negligible, but this difference became greater as the impact energy became higher: namely, the improvement in impact damage resistance due to the stitching became greater as the impact energy increased.

Figures 5 and 6 show micro-focus X-ray CT images of unstitched and stitched specimens, where white lines indicate cracks. Sections (s1)–(s5) in the Figs 5 and 6 correspond to the (s1)–(s5) in the Fig. 3. In both stitched and unstitched specimens, delamination, which is indicated by a horizontal white line, occurred at each interface and ply cracks, which are indicated by a vertical white line, connected the delaminations. The damage distributions in through-the-thickness direction were different between stitched and unstitched specimens. In the unstitched specimen, damage became gradually greater from the top to the bottom of the specimen, and the greatest damage occurred at the bottom of the specimen. In contrast, in the stitched specimen, the damage became greater from the top to the center of the specimen, and the damage then became progressively less from the center to the bottom. The greatest damage was located around the center of the specimen.

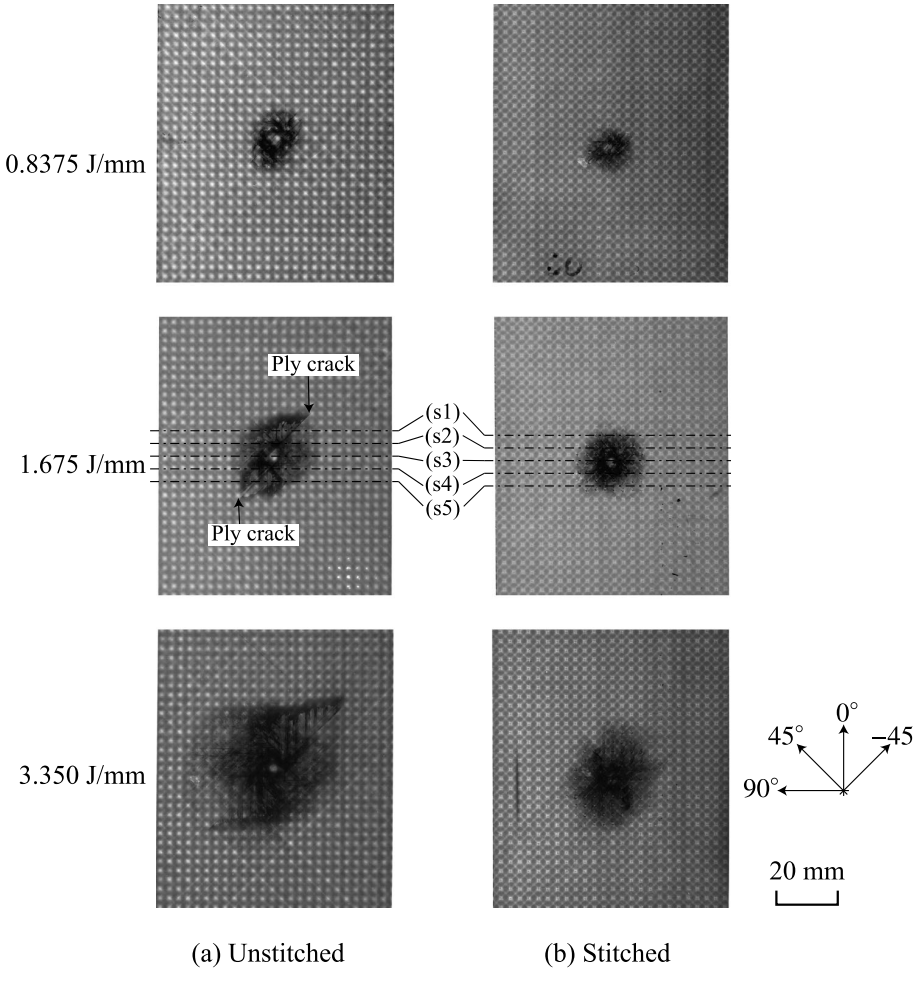

Figure 3. Soft X-ray radiographs of the impacted specimens.

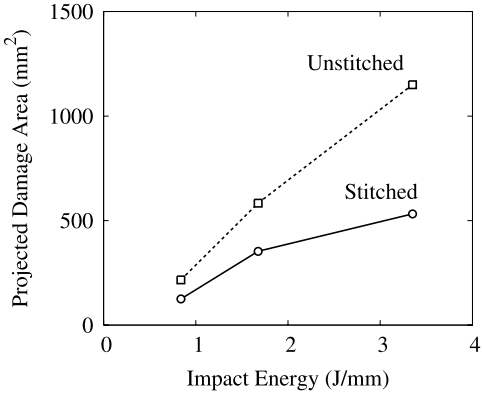

Figure 4. Projected area of measured impact damage as a function of impact energy.

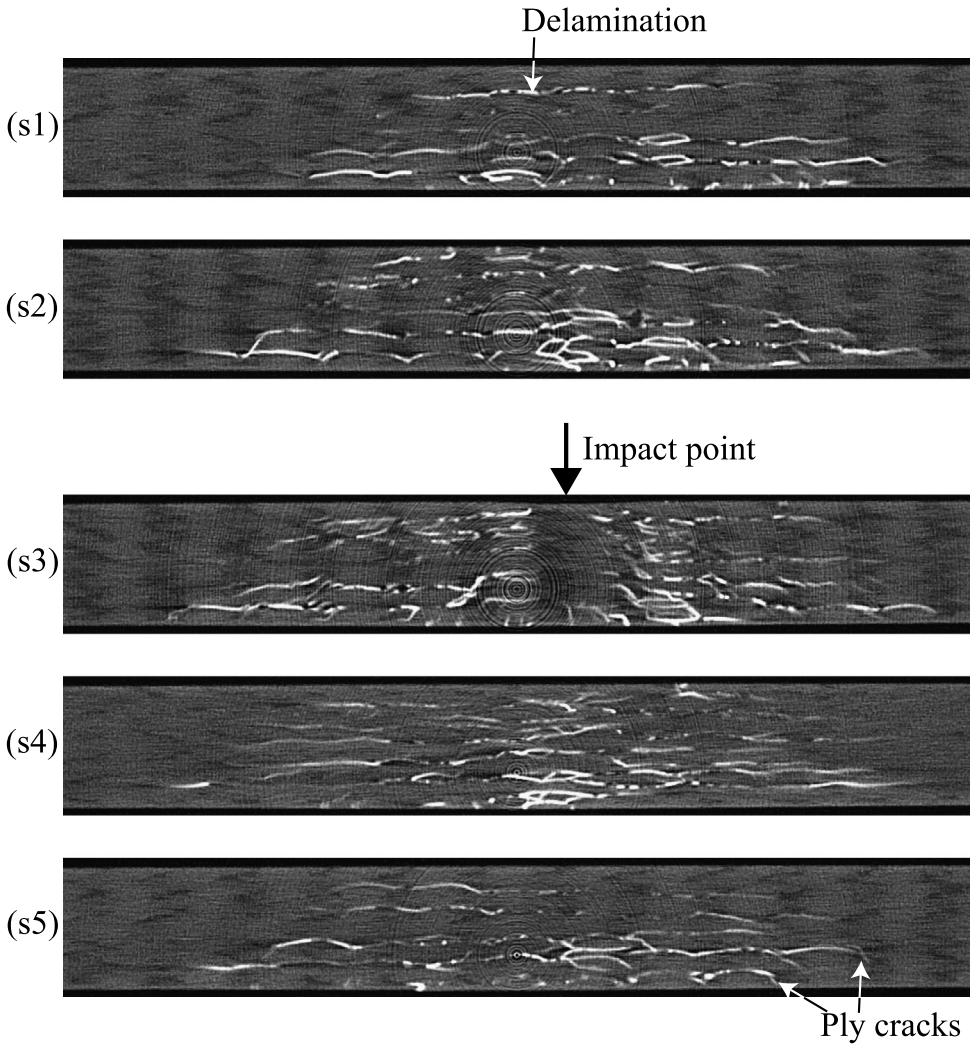

Figure 5. Soft X-ray CT images of the unstitched specimen. White line indicates the crack penetrated by contrast medium (zinc iodide).

3. Analysis

3.1. Simulation Model

The impact velocity of the experiment was about 1.0–3.0 m/s. Therefore, we regarded the impact events as low velocity impact [18]. Generally, the low velocity impact load and the static indentation load cause almost identical damage in the CFRP laminates [19]. Therefore, in the present simulation, the static indentation load was applied to the finite element model, and the energy release rate of each interface was calculated by the virtual crack closure technique (VCCT).

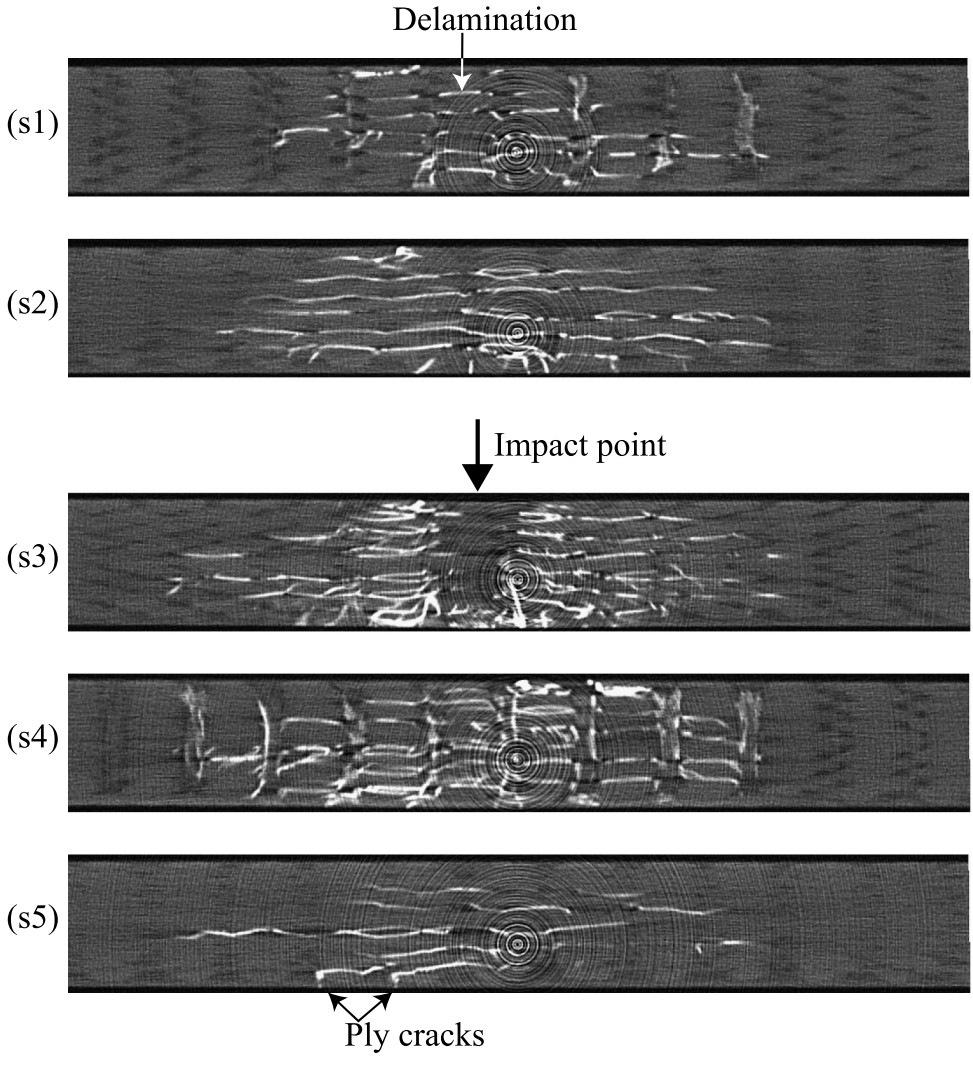

Figure 6. Soft X-ray CT images of the stitched specimen.

Figure 7 provides an overview of the finite element model. The stacking sequence was $[-45/0/45/90]_{3s}$, the same as in the experiment. The model was divided by 15-node and 20-node isoparametric solid elements. Each ply was expressed by one element in the thickness direction except for the 90° plies located at the center. These two plies were expressed by one element.

Circular initial delamination was introduced at each interface except for the 90°/90° interface at the center of the thickness direction (Fig. 7b). The diameter of the delamination d was varied: 4.0, 11.0, 16.5 and 22.0 mm. The mesh of the model was slightly different depending on the diameter d (Fig. 7c). We considered a single crack at every ply because a single long ply crack occurred in the bottom

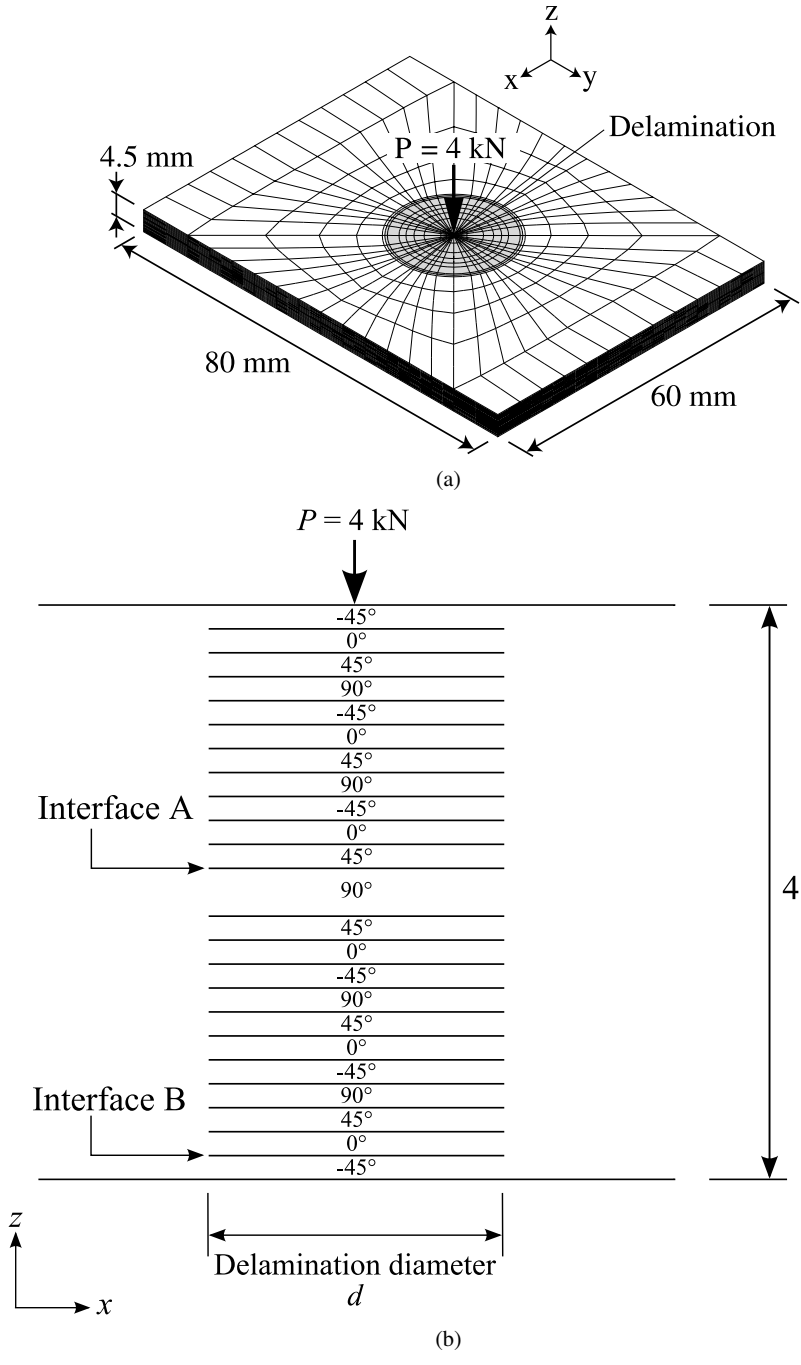

Figure 7. Finite element model for energy release rate calculation. (a) Overview of the mesh, (b) schematic of the delamination, (c) delamination and arrangement of spring elements, (d) ply crack arrangement of each layer.

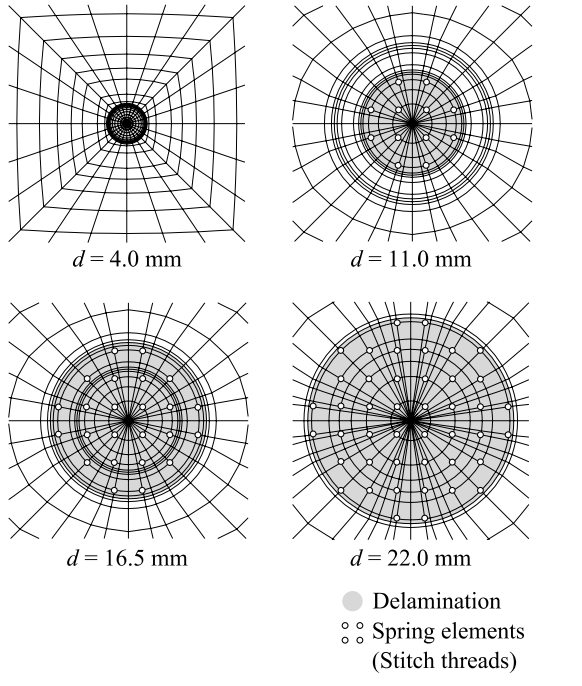

(c)

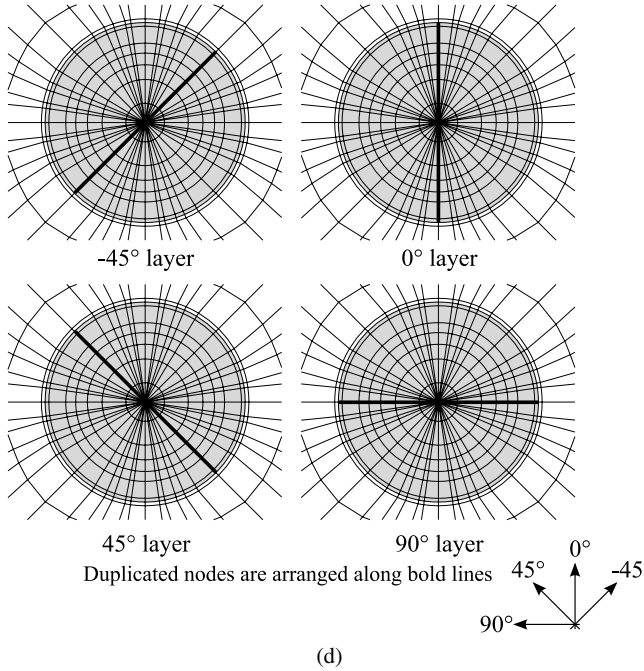

(d)

Figure 7. (Continued.)

surface of the specimen in the experiment. The length of the crack was the same as the diameter of the initial delamination, and the crack was parallel to the fiber orientation. Figure 7d shows the crack arrangement of each layer, where the diameter of the delamination d was 22.0 mm. The delamination and ply cracks were expressed by duplicated nodes. We considered the contact of the crack surfaces by introducing penalty spring elements which generate reaction force only when surface nodes overlap.

In the stitched laminate, the stitch threads affect the stiffness in the through-the-thickness direction. Moreover, after onset of the delamination, the threads bridge the delamination, and generate a crack closure force. We considered the effect on the stiffness by superimposing the stiffness of the thread onto the stiffness of the laminate. In order to consider the bridging effect, we introduced linear spring elements that connect the neighboring layer. The arrangement of the spring is shown in Fig. 7c. The stiffness of the spring elements was determined from the literature [20] describing composite rod pull-out tests. In the present model, we did not consider the nonlinear behavior of the bridging force because the crack opening displacement was sufficiently small. The stiffness of the spring was 2.25×10^2 N/mm in the mode I direction and 3.75×10^2 N/mm in the mode II direction.

We prepared two models including the stitched model, in which the stitching effects were considered, and the unstitched model, in which the stitching effects were not considered. Four edges of the model were clamped, and a concentrated load (4 kN) was applied along the $-z$ direction. The energy release rate along the delamination front at each ply interface was calculated from the displacement and nodal force of the crack tip.

3.2. Simulation Results

For the analysis, commercial finite element code ABAQUS 6.6-1 was employed. Table 1 presents the material properties used in the present analysis, where subscript L denotes fiber direction, and T indicates transverse direction. Figure 8 plots the in-plane energy release rate distributions of interface A and interface B which were indicated in Fig. 7b when the delamination diameter d equaled 22.0 mm. Interface A is the eleventh interface from the top, and interface B is the twenty second. The radial coordinate (r) indicates the energy release rate, and the circumferential

Table 1.
Material properties of a single ply

Longitudinal Young's modulus E_L (GPa)	149.83
Transverse Young's modulus E_T (GPa)	7.65
Longitudinal shear modulus G_{LT} (GPa)	3.25
Transverse shear modulus G_{TT} (GPa)	2.57
Longitudinal Poisson's ratio υ_{LT}	0.281
Transverse Poisson's ratio υ_{TT}	0.177

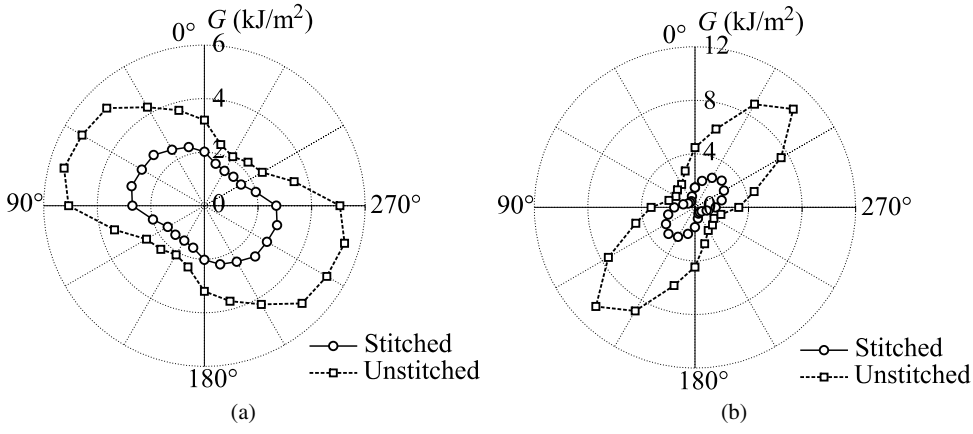

Figure 8. In-plane energy release rate distributions of (a) interface A (45°/90°) and (b) interface B (0°/−45°).

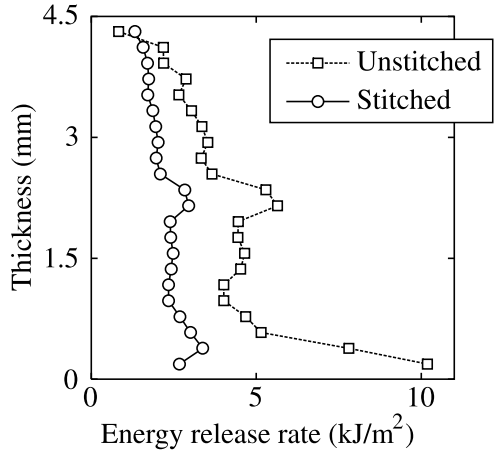

Figure 9. Through-the-thickness distribution of energy release rate.

coordinate (θ) indicates the direction of crack extension. The direction where the energy release rate reached its peak value was dependent on the fiber directions of neighboring layers. The energy release rate of the stitched model was lower than that of the unstitched one.

The maximum energy release rate of each interface is plotted in Fig. 9. The vertical axis indicates the position of the interface in the thickness direction. The indentation load was applied at $z = 4.5$ mm. The energy release rate of the stitched model was always lower than that of the unstitched model. In the unstitched model, the energy release rate progressively increased from the top to the center of the model. After it peaked at the center of the model, it sharply increased around the bottom of the model (opposite surface to the impacted surface). On the other hand, in the stitched model, although there were small peaks at the center and the bottom

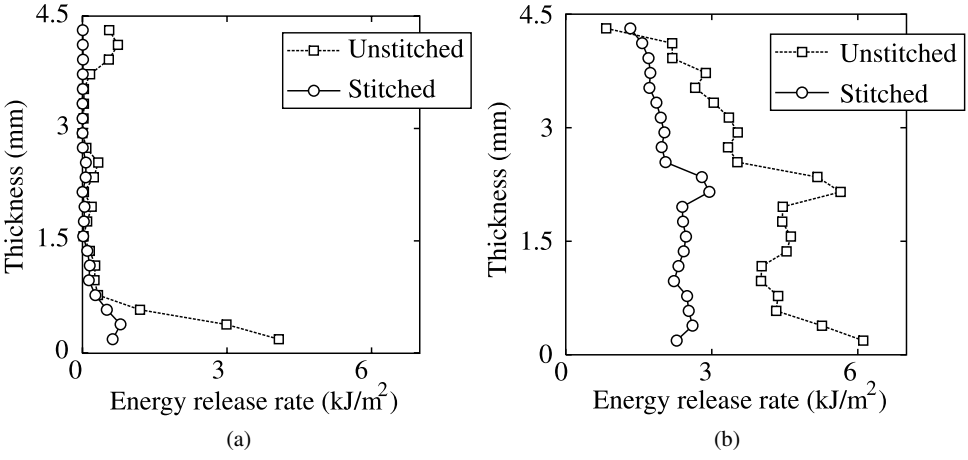

Figure 10. Modes I and II components of energy release rate.

of the model, the peak at the bottom of the model was much lower than that in the unstitched model. These results clearly explain the experimental results (Figs 5 and 6).

Figure 10 plots separately the through-the-thickness distribution of the modes I and II component of the energy release rate. The mode I component of the energy release rate of the unstitched model sharply increased around the bottom of the model because the indentation load caused peel deformation of the bottom layer. In the stitched model, on the other hand, the mode I component of the energy release rate remained consistently low. Moreover, in the stitched model, the mode II component of energy release rate was lower, especially from the center to the bottom of the model. In the bottom of the model, the reductions of modes I and II were superimposed. We conclude that the stitching affected the through-the-thickness distribution of the impact damage because the stitching strongly suppressed the peel deformation and shear deformation at the bottom of the laminate.

The relationship between the delamination diameter and maximum energy release rate is shown in Fig. 11, where the maximum energy release rate means the maximum value of the energy release rate throughout the entire model. The energy release rate of the unstitched model saturated as the delamination diameter increased. In the stitched model, on the other hand, it decreased as the delamination diameter increased, because the larger delamination contained more stitch threads bridging the delamination. These results confirm the experimental results that the improvement in impact damage resistance due to stitching became more pronounced as the impact energy became higher (Fig. 4). Higher impact energy causes greater delamination. However, as delamination grows larger, the energy release rate decreases in the stitched laminate. Therefore, in the stitched laminate, the energy needed for the same amount of delamination growth becomes larger as the impact energy increases. As a result, the difference of impact damage between the stitched and unstitched laminates grows larger as the impact energy increases.

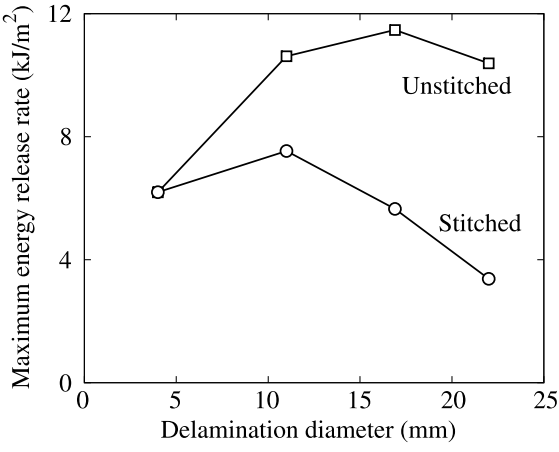

Figure 11. Relationship between maximum energy release rate and delamination diameter d.

The above results and discussion imply that the variations in impact energy cause major variations in the degree to which out-of-plane damage resistance is improved. We conclude that the variation in the impact energy accounts for the varying degrees of damage resistance improvement seen in the literature.

4. Conclusion

The present paper experimentally and numerically investigated the out-of-impact damage in stitched laminates, and revealed the effect of stitching on the out-of-plane impact damage resistance.

1. Both experimental and numerical results demonstrated that the out-of-plane impact resistance of CFRP laminates was improved by stitching. The improvement in damage resistance became greater when the impact energy was higher.
2. The stitching affected the through-the-thickness damage distribution. The numerical results demonstrated that this was because stitching strongly suppressed both peel (mode I) and shear (mode II) deformations around the bottom of the laminates.
3. Simulation results revealed that the improvement in impact damage resistance due to stitching became greater as the delamination area grew larger. This caused the improvement in out-of-plane impact damage resistance to become greater when impact energy was higher.

Acknowledgement

A. Yoshimura is supported by the Ministry of Education, Culture, Sports, Science and Technology of Japan under a Grant-in-Aid for Scientific Research (No. 16 · 11471).

References

1. L. Tong, A. P. Mouritz and M. K. Bannister, *3D Fiber Reinforced Polymer Composites*. Elsevier Science Ltd., Oxford, UK (2002).
2. K. Dransfield, C. Baillie and Y. W. Mai, Improving the delamination resistance of CFRP by stitching — a review, *Compos. Sci. Technol.* **50**, 305–317 (1994).
3. L. Jain and Y. W. Mai, On the effect of stitching on mode I delamination toughness of laminated composites, *Compos. Sci. Technol.* **51**, 331–345 (1994).
4. L. Jain and Y. W. Mai, Determination of mode II delamination toughness of stitched laminated composites, *Compos. Sci. Technol.* **55**, 241–253 (1995).
5. A. P. Mouritz, J. Gallagher and A. A. Goodwin, Flexural strength and interlaminar shear strength of stitched GRP laminates following repeated impacts, *Compos. Sci. Technol.* **57**, 509–522 (1997).
6. F. Larsson, Damage tolerance of a stitched carbon/epoxy laminate, *Composites Part A* **28A**, 923–934 (1997).
7. K. A. Dransfield, L. K. Jain and Y. W. Mai, On the effects of stitching in CFRPs — I. Mode I delamination toughness, *Compos. Sci. Technol.* **58**, 815–827 (1998).
8. L. K. Jain, K. A. Dransfield and Y. W. Mai, On the effects of stitching in CFRPs — II. Mode II delamination toughness, *Compos. Sci. Technol.* **58**, 829–837 (1998).
9. Y. Iwahori, T. Ishikawa, Y. Hayashi and N. Watanabe, Study of interlaminar fracture toughness improvement on stitched CFRP laminates, *J. Japan Soc. Compos. Mater.* **26**, 90–100 (2000).
10. A. P. Mouritz, Ballistic impact and explosive blast resistance of stitched composites, *Composites Part B* **32B**, 431–439 (2001).
11. Y. Iwahori, S. Sugimoto, Y. Hayashi, S. Horikawa, T. Ishikawa and H. Fukuda, Study of mechanical properties under through-the-thickness loads for stitched CFRP laminates by using tension test specimens with a single stitch thread, *J. Japan Soc. Compos. Mater.* **32**, 22–31 (2006).
12. D. Liu, Delamination resistance in stitched and unstitched composite plates subjected to impact loading, *J. Reinf. Plast. Compos.* **9**, 59–69 (1990).
13. E. Wu and J. Liau, Impact of unstitched and stitched laminates by line loading, *J. Compos. Mater.* **28**, 1640–1658 (1994).
14. E. Wu and J. Wang, Behavior of stitched laminates under in-plane tensile and transverse impact loading, *J. Compos. Mater.* **29**, 2254–2279 (1995).
15. M. V. Hosur, M. Adya, J. Alexander, S. Jeelani, U. Vaidya and A. Mayer, Studies on impact damage resistance of affordable stitched woven/epoxy composite laminates, *J. Reinf. Plast. Compos.* **22**, 927–952 (2003).
16. I. Herszberg and T. Weller, Impact damage resistance of buckled carbon/epoxy panels, *Compos. Struct.* **73**, 130–137 (2006).
17. R. Kamiya, B. A. Cheeseman, P. Popper and C. T. Wei, Some recent advantages in the fabrication and design of three-dimensional textile preforms: a review, *Compos. Sci. Technol.* **60**, 33–47 (2000).
18. M. O. W. Richardson and M. J. Wisheart, Review of low-velocity impact properties of composite materials, *Composites Part A* **27A**, 1123–1131 (1996).
19. A. T. Nettles and M. J. Douglas, A comparison of quasi-static indentation to low-velocity impact, NASA TP-2000-210481 (2000).
20. D. D. R. Cartie, B. N. Cox and N. A. Fleck, Mechanisms of crack bridging by composite and metallic rods, *Composites Part A* **35A**, 1325–1336 (2004).